Crystal Structure of *Escherichia coli* MscS, a Voltage-Modulated and Mechanosensitive Channel

Randal B. Bass,[1] Pavel Strop,[2] Margaret Barclay,[3] Douglas C. Rees[1,3]*

The mechanosensitive channel of small conductance (MscS) responds both to stretching of the cell membrane and to membrane depolarization. The crystal structure at 3.9 angstroms resolution demonstrates that *Escherichia coli* MscS folds as a membrane-spanning heptamer with a large cytoplasmic region. Each subunit contains three transmembrane helices (TM1, -2, and -3), with the TM3 helices lining the pore, while TM1 and TM2, with membrane-embedded arginines, are likely candidates for the tension and voltage sensors. The transmembrane pore, apparently captured in an open state, connects to a large chamber, formed within the cytoplasmic region, that connects to the cytoplasm through openings that may function as molecular filters. Although MscS is likely to be structurally distinct from other ion channels, similarities in gating mechanisms suggest common structural elements.

The mechanosensitive channel of small conductance, MscS, was identified by Kung and co-workers (*1*) as a stretch-activated channel present in the inner membrane (*2*) of *E. coli*. The MscS channel is characterized by a conductance of ~1 nS, with a slight preference for anions; this is substantially larger than the conductances of typical eukaryotic ion channels (1 to 30 pS) (*3*) but smaller than the ~3 nS, nonselective conductance observed for the prokaryotic MscL (large conductance) mechanosensitive channel (*4*). Both MscS and MscL are intrinsically mechanosensitive, opening in response to stretching of the cell membrane without the requisite participation of cytoskeletal or other components. The pressure threshold for MscS opening is ~50% that of MscL, which in turn opens at pressures near the rupture point of the bilayer (*1, 5*). The properties of these channels likely reflect their involvement in the cellular response to rapid decreases in external osmolarity (*6–9*), and the two channels share the ability to partially compensate for the deletion of the other (*8*). The gene encoding the MscS channel, *yggB*, was identified by Booth and co-workers (*8*); the *E. coli* protein, with 286 amino acids (see fig. S1) is predicted from hydropathy analyses to have three transmembrane helices (*10*) and exhibits no detectable sequence similarities to the smaller (136 residues) MscL. In common with MscL (*4, 11*) and other prokaryotic channels such as KcsA (*12*), MscS exists as a homo-oligomer (*5, 13*). However, MscS has a far greater distribution than MscL (fig. S2) throughout eubacteria and has also been identified in Archaea and at least some eukaryotes (*8, 14*).

The conductances of gated channels such as MscS are regulated by conformational switching of the protein structure between open and closed states. This switching responds to changes in environmental conditions, including applied tension (mechanosensitive channels), variation in membrane potential (voltage-gated channels), and binding of ligands (ligand-gated channels). In recent years, progress has been made in defining the structural basis of channel gating. After the structure of the closed state of MscL was determined (*11*), detailed models were described for the structure of the open state and the coupling between membrane tension and structure (*15–18*). Structural aspects of the mechanism of ligand gating have been established for opening a prokaryotic potassium channel (*12*) by proton binding to the channel (*19*) and by calcium binding to an extramembrane domain (*20, 21*). Although considerable insights into the mechanism of voltage-dependent gating have been achieved [see (*3, 22*)], to date, no structures of a voltage-gated system have been described. The properties of MscS bear on two important issues related to channel gating: (i) although MscS and MscL are not evidently homologous, they are functionally similar, providing the opportunity to identify common structural features that may be relevant to mechanosensitivity; (ii) in addition to mechanosensitivity, the open probability of MscS is significantly increased by membrane depolarization (*1, 9*). The open probability of MscS increases *e*-fold for each +15 mV (*1, 5, 9*), which is equivalent to the effective movement of ~1.7 charges [see (*3*)] across the membrane during the transition from the closed to the open states. To provide a framework for understanding the conductance properties, we have determined the structure of the *E. coli* MscS at 3.9 Å resolution and suggest a mechanism for the gating process. The coordinates have been deposited in the Protein Data Bank (1MXM) for release upon publication.

[1]Division of Chemistry and Chemical Engineering, [2]Biochemistry Option, [3]Howard Hughes Medical Institute, Mail Code 114-96, California Institute of Technology, Pasadena, CA 91125, USA.

*To whom correspondence should be addressed. E-mail: dcrees@caltech.edu.

Structure Determination of MscS

We obtained crystals of *E. coli* MscS following a strategy similar to that used for MscL (*11*) of screening multiple homologs and detergents to identify sequences and solubilization conditions that yield crystals of quality suitable for diffraction analysis (*23*). The initial electron density maps were calculated with multiwavelength anomalous diffraction phases obtained from data recorded at the selenium edge from selenomethionine-substituted MscS crystals, and they were improved by sevenfold noncrystallographic symmetry averaging (Fig. 1). The quality of the resulting electron density map at 3.9 Å resolution was excellent and allowed the modeling and sequence assignment of the polypeptide chain; for this purpose, the positions of the selenomethionines served as important markers. At this resolution, however, unambiguous placement of all side chains and identification of hydrogen bonds is not possible. All but the first 26 and the last 6 residues of the 286 amino acids in MscS have been modeled, with density present for virtually the entire main chain and all but 17 side chains (assigned occupancies of 0 in the PDB file). The final R/R_{free} values of 0.33 and 0.36 were obtained from a single model, with no disallowed residues in the Ramachandran plot. Although high, these R values reflect the modest resolution of the structure, particularly the sharp decrease in intensity of the diffraction pattern with resolution. Table 1 summarizes the data collection, phasing, and refinement statistics for the MscS structure determination.

Structural Organization of MscS

The crystal structure of MscS establishes that this channel folds as a homoheptamer of approximate cylindrical shape (Fig. 2). Architecturally, MscS can be divided into transmembrane and extramembrane regions; the latter can be further divided into two domains designated middle-β and COOH-terminal. In overall dimensions, MscS extends for ~120 Å parallel to the sevenfold axis, with the membrane and extramembrane domains accounting for ~50 Å and 70 Å, respectively, while the width in the perpendicular direction spans ~80 Å. On the basis of fusion experiments reported for *yggB* and the homologous protein KefA (*10*), it is likely that the extramembrane region is cytoplasmic and that the NH_2-terminus of MscS is periplasmic.

Helices from the membrane-spanning region form a channel through the membrane coincident with the sevenfold axis that opens into to an ~40 Å–diameter chamber enclosed by the extramembrane portions of the MscS subunits. This chamber is connected in turn to the cytoplasm through eight portals between the middle-β and COOH-terminal domains of each subunit. At all levels, the structural organization of MscS is completely distinct from that of MscL or any other structurally characterized channel.

The transmembrane domain of each subunit contains three membrane-spanning helices, designated TM1 (residues 29 to 57), TM2 (residues 68 to 91), and TM3 (residues 96 to 127, with a pronounced kink at residue 113 that likely marks the membrane boundary). The helices are tilted by 27° to 35° with respect to the membrane normal (defined as the direction of the sevenfold axis), typical of the values observed for the KcsA and MscL channels (*11, 12*). The channel pore extends along the center of this domain and is formed principally by residues 96 to 113 of the TM3 helices that should span the cytoplasmic half of the membrane (the inner leaflet of the lipid bilayer) with the loop connecting TM2 and TM3 extending through the periplasmic side of the bilayer. The apparent direction of the TM3 polypeptide chain across the membrane, with the COOH-terminus in the cytoplasm (*10*), is identical to that observed for the pore-forming helices in KcsA but opposite that observed in MscL. Flanking the TM3 pore along the periphery of the transmembrane domain are pairs of TM1-TM2 helices. Although the two helices from each subunit are closely packed, they appear to be displaced from the core of TM3 helices and the density is less well defined, suggesting that they are more conformationally mobile than the rest of the protein. Residues 92 to 95, which connect the TM2 and TM3 helices, adopt an extended conformation that contributes to the pore, while TM3 proceeds through the membrane to the cytoplasmic surface. After a sharp kink at Gly^{113}, the helical axis becomes oriented nearly parallel to the plane of the putative lipid bilayer. It appears plausible that this COOH-terminal region of TM3 either sits in or is adjacent to the head group region of the bilayer. The relatively high degree of sequence conservation in the TM3 helix (*8*) (fig. S1) highlights the importance of this region for MscS function.

The extramembrane region of MscS surrounds a large water-filled chamber of ~40 Å diameter. The two domains of each subunit that constitute this part of the protein, middle-β and COOH-terminal, create a framework for this enclosure that connects to the cytoplasm through eight openings. The middle-β domain (residues 132 to 177) contains five β strands that pack together with those of the other subunits to form an essentially continuous barrel-like β sheet that extends around the entire protein. The COOH-terminal domain of the protein (residues 188 to 265) exhibits a mixed α/β structure with four strands, β6 to β9, and two α helices. Two of these strands, β6 and β7, form a nearly a continuous strand, with a break at residue Phe^{188}. The two α helices pack against an antiparallel sheet formed from these β strands. Seven of the openings leading into this chamber are framed by the middle-β and COOH-terminal domains to form portals of ~14 Å diameter. Completing the structure, all seven subunits are linked together through a seven-stranded parallel β barrel at the COOH terminus of MscS that contains one strand, β10, from each subunit. The opening through the center of this barrel, the eighth into the chamber, has a diameter of ~8 Å.

Properties of the Pore

The TM3 helices of each subunit line the transmembrane pore and are packed together with crossing angles of −22° to form a right-handed bundle, as observed in other channels (*24*). Due to the presence of conserved glycines at positions 101, 104, and 108, adjacent TM3 helices interact tightly, with an interhelical distance of ~8 Å. As a consequence of this arrangement, the permeation pathway resembles a tapered cylinder, with a diameter of ~11 Å at the closest contact point (Fig. 3). This constriction near the cytoplasmic surface of the membrane-spanning region is created by the side chains of Leu^{105} and Leu^{109}. A mutation at position 922 in the homologous protein KefA (*10*), corresponding to residue Ala^{106} in MscS, has been reported to produce a channel that is more sensitive to pressure (*25*) and cells that are hypersensitive to potassium (*10*), underscoring

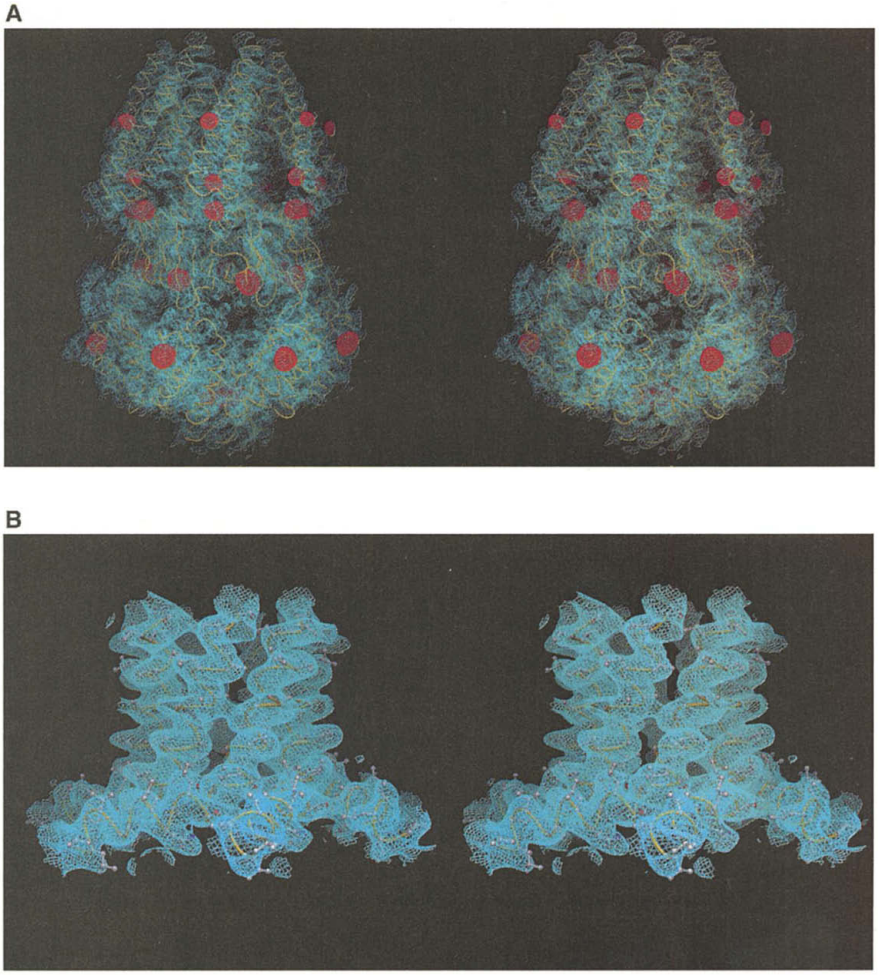

Fig. 1. Stereoviews of electron density maps. (**A**) Experimental electron density map surrounding the entire MscS protein. Backbone atoms are traced in yellow, with the 3.9 Å resolution experimental density map contoured at 1.0σ. For this calculation, the observed structure factor amplitudes were sharpened by an overall $B = -75$ Å^2 applied before sevenfold NCS averaging. The anomalous difference Fourier map calculated from the selenomethionine-substituted data is contoured at 4.0σ in red. (**B**) Expanded stereoview of the experimental density (contoured at 1.0σ) surrounding the transmembrane pore (TM3 helices). The α-carbon trace is illustrated in yellow for residues 95 to 125, with side chains rendered as ball and stick. This figure was prepared with the program DINO (www.biozentrum.unibas.ch/~xray/dino).

the functional importance of this region of the channel.

As MscS adopts at least two conformations (closed and open) with different conductances, the correspondence between the structure and functionally characterized states needs to be established. The conductance of MscS is ~1 nS at neutral pH (MscS crystals were grown at pH 7.2), although it decreases significantly at lower pH values (*9*). From an analysis of the relationship between conductance and pore dimensions in structurally characterized channels (*26*), it appears that a conductance of ~1 nS requires a minimum pore diameter of ~8 Å [although larger diameters (~16 Å) have also been discussed for MscS (*5*)]. Because the observed diameter of the MscS pore (~11 Å) is within this range, and much larger than observed for the structure of MscL assigned to the closed state (*11, 17*), it is likely that the structure reflects the open state of MscS. Although the closed state of MscS is favored in the membrane by ~7 kcal/mol in the absence of applied tension (*5*), apparently the lateral pressures (*17, 27, 28*) required to maintain this state are not provided in the detergent micelles of Foscholine-14 used to solubilize MscS for the structure determination.

In contrast to the polar residues lining the permeation pathway in MscL, the MscS pore is largely apolar, with the exception of Ser^{95} at the NH_2-terminus of TM3. Overall, the electrostatic potential for the entire transmembrane domain is surprisingly positive (Fig. 3) because of the presence of several arginines, most notably at residues 46 and 74, in the membrane-spanning helices as well as Arg^{88} of TM2, which points into the pore. These electrostatic effects may contribute to the slight preference exhibited by MscS for the conductance of anions relative to cations (~3 Cl^- ions for 2 K^+ ions) (*1, 13*).

On the intracellular side of the channel, the permeation pathway of MscS does not connect directly to the cytoplasm but, as discussed above, instead opens to a large chamber that is connected to the exterior through eight openings of diameters of ~8 to 14 Å. The organization of this assembly resembles a molecular filter that could serve to prescreen large molecules before they are allowed passage to the transmembrane pore; an analogous role has been proposed for the intracellular domain of the acetylcholine receptor (*29*).

Gating Transition of MscS

The equilibrium between closed (C) and open (O) states of MscS can be shifted toward the latter by a combination of tension applied to the membrane or depolarization of the membrane potential. In terms of a simple, two-state model, C ↔ O, the protein conformation can be thermodynamically coupled to these changes in applied tension or membrane potential if the transition from the closed to the open state is associated with both a larger cross-sectional area (*30*) and a net movement of positive charge across the membrane toward the periplasm (*31*). Analysis of the gating transition of MscS indicates that, relative to the closed state, the open state exhibits an increase in cross-sectional area of 840 $Å^2$ (*5*) and the equivalent to the movement of about +1.7 charges completely across the membrane (*1*). [This effect is more realistically accomplished by moving a greater number of charges proportionally shorter distances across the membrane; see (*3*)]. The tension and voltage sensitivities are coupled (*1, 9*) so that, as the membrane is depolarized, less tension is required to open the channel and vice versa.

Whereas the permeation pathway is clearly formed from the TM3 helices and the connecting loop from TM2, the TM1 and TM2 helices appear to be likely candidates for mediating the tension and voltage sensitivities of MscS. The TM1 and TM2 helices are closely packed in

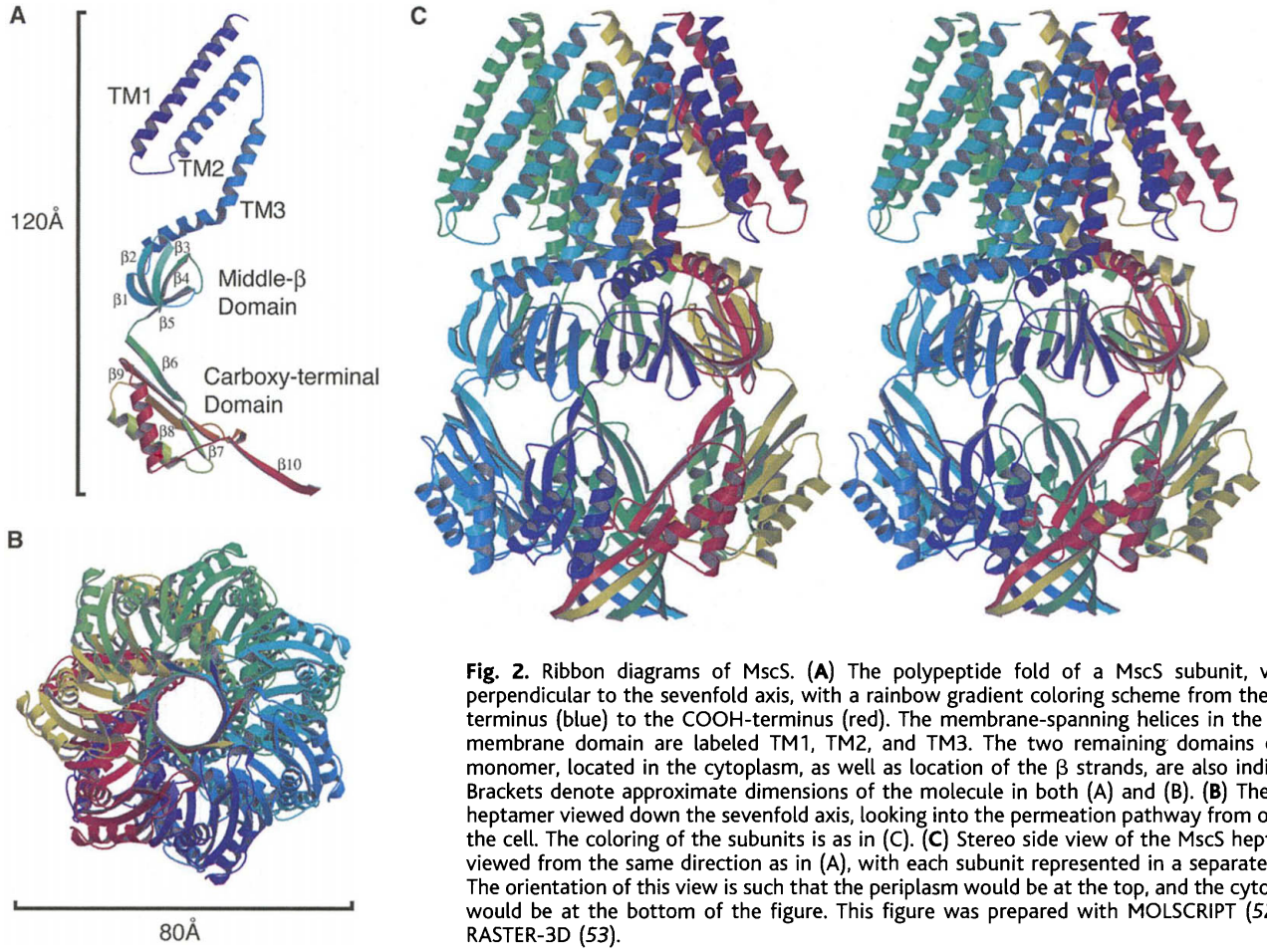

Fig. 2. Ribbon diagrams of MscS. (**A**) The polypeptide fold of a MscS subunit, viewed perpendicular to the sevenfold axis, with a rainbow gradient coloring scheme from the NH_2-terminus (blue) to the COOH-terminus (red). The membrane-spanning helices in the transmembrane domain are labeled TM1, TM2, and TM3. The two remaining domains of the monomer, located in the cytoplasm, as well as location of the β strands, are also indicated. Brackets denote approximate dimensions of the molecule in both (A) and (B). (**B**) The MscS heptamer viewed down the sevenfold axis, looking into the permeation pathway from outside the cell. The coloring of the subunits is as in (C). (**C**) Stereo side view of the MscS heptamer, viewed from the same direction as in (A), with each subunit represented in a separate color. The orientation of this view is such that the periplasm would be at the top, and the cytoplasm would be at the bottom of the figure. This figure was prepared with MOLSCRIPT (*52*) and RASTER-3D (*53*).

nearly antiparallel fashion (crossing angle = 165°, with an interhelical distance of 9 Å), and they are displaced from the core of TM3 helices in the transmembrane region. The positioning of the TM1 and TM2 helices at the periphery of the membrane-spanning region of MscS suggests they could change their orientation in response to applied tension, with an accompanying change in cross-sectional area that could serve as the sensor for coupling tension to conformational changes. Furthermore, TM1 and TM2 both contain arginines, at positions 46 and 74, respectively, that are spatially adjacent to each other and are near the middle of the likely membrane-spanning region where they would be appropriately sited to respond to changes in membrane potential. Arginines 54, 59, and 88 and lysine 58 are positioned near the membrane-water interface and could also possibly play a role in voltage sensing. The isolation by Blount and co-workers (*32*) of apparent gain-of-function mutants in MscS located in TM1 (the substitution of Asp or Lys for Val^{40}) underscores the sensitivity of channel function to the presence of charged residues in this region. Consequently, the combined presence of these charged residues and the location of the TM1 and TM2 helices adjacent to the permeation pathway indicate that TM1 and TM2 are likely candidates for mediating the conformational response of MscS to changes in either applied tension or membrane depolarization.

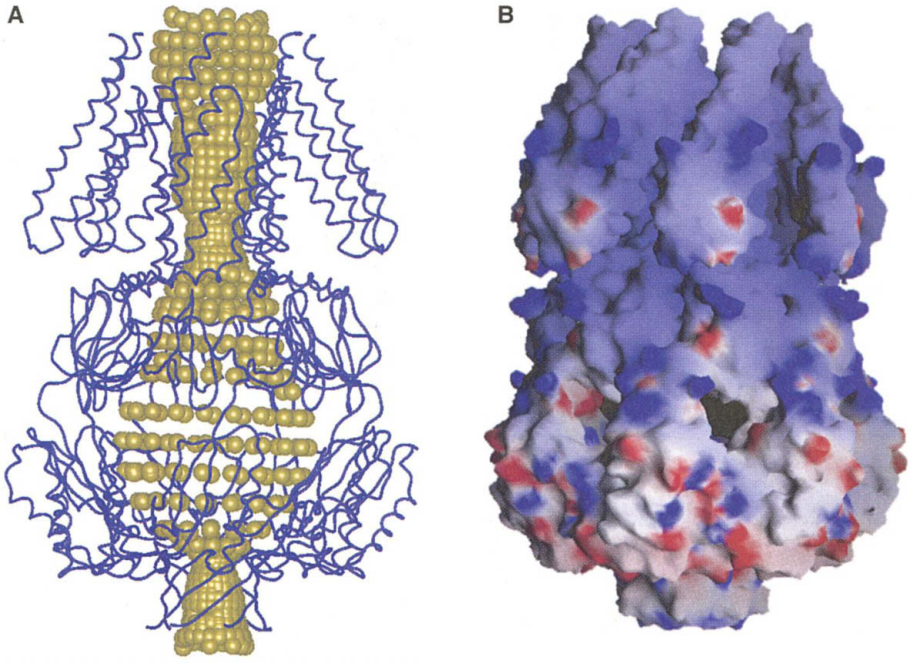

Fig. 3. HOLE diagram and electrostatic potential surface of MscS. (**A**) Ribbon diagram of MscS superimposed on probe spheres outlining the permeation pathway, as calculated by using HOLE (*54*). The position of the yellow probe spheres illustrates the path ions and water could take when passing through the channel. The portals through the extramembrane domain that connect the interior chamber with the exterior are not identified in this calculation. (**B**) GRASP (*55*) surface of the MscS channel calculated with the DELPHI (*56*) electrostatic potential. The blue, white, and red shadings represent positively charged (+15 kT), neutral, and negatively charged (−15 kT) surface regions, respectively. The channel is viewed normal to the sevenfold axis, with the cytoplasmic region at the bottom, as in Fig. 2 (A and C).

An attractive mechanism for gating MscS involves reorientation of the TM1 and TM2 helices with respect to TM3 (Fig. 4). With a pivot point near the extracellular side of the protein, movement in these helices between open and closed states in response to mechanical stress would necessarily move the arginine residues present on TM1 and TM2 within the membrane. The observed sensitivity of channel opening to membrane potential, corresponding to the transmembrane movement of 1.7 charges, is equivalent to 14 charges (2 per subunit) moving ~1.7/14 = 0.12 of the way across the membrane. For a membrane

Table 1. Summary of data collection, phasing, and refinement statistics. Crystals of MscS were grown [see (*23*)] in space group $P4_32_12$ with cell dimensions $a = b = 184.7$ Å, $c = 260.7$ Å and contain one heptameric MscS channel per asymmetric unit. All data were collected at −170°C on beamline 9-2 at SSRL with an Area Detector Systems Corportion charge-coupled device detector and processed with DENZO/SCALEPACK (*45*). Initial positions of the selenium sites were obtained by SOLVE (*46*), with subsequent refinement of the sites and phase calculation with SHARP (*47*). Density modification with solvent flattening and sevenfold noncrystallographic symmetry averaging was carried out with DM (*48*); the model was built with O (*49*) and refined with CNS (*50*). Structure factor sharpening (with an applied *b*B factor of –75 Å^2) was used only for map calculations. The stereochemical quality of the model was verified with PROCHECK (*51*), which indicated that 94.2% of residues were in the most favored and additionally allowed regions of the Ramachandran plot, and none were disallowed. MAD, multiwavelength anomalous diffraction, rmsd, root-mean-square deviation.

	Native	Peak	Inflection	Remote
Wavelength (Å)	1.009	0.9788	0.9791	0.9184
Resolution (Å)	30–3.9	40–5.0	40–5.0	30–5.0
Unique reflections	44094	19486	19321	19475
Redundancy	15.1	17.6	6.78	7.34
Completeness	99.9 (99.4)	99.8 (99.5)	99.1 (96.7)	99.4 (99.2)
I/σ	24.9 (4.5)	29.6 (6.2)	23.1 (2.7)	28.8 (4.1)
R_{merge}	0.091 (0.41)	0.087 (0.46)	0.074 (0.49)	0.065 (0.43)

Phasing, selenomethionine MAD	
Resolution (Å)	30–5.0
Number of sites	42
Anomalous phasing power, peak (acentric)	3.45
Isomorphous phasing power, inflection (centric/acentric)	0.497/0.756
Anomalous phasing power, inflection (acentric)	2.20
Isomorphous phasing power, remote (centric/acentric)	0.842/1.27
Anomalous phasing power, remote (acentric)	2.16

Refinement against native	
Resolution (Å)	15–3.9
Reflections used	40888
Number of nonhydrogen atoms	13573
R_{work}	0.329 (0.399)
R_{free}	0.356 (0.405)
$B_{average}$ (Å^2)	125.5
rmsd bond length (Å)	0.011
rmsd bond angle (°)	1.3

20 Å thick [the approximate width of the most nonpolar region of membranes (*33*)], this will require a movement of ~2.4 Å per charge. Conformational changes of this magnitude could be achieved, for example, by the pivoted motion of the TM1 and TM2 helices closer or farther from the channel axis in the closed, or open state, respectively. Rearrangements of this type not only would change the cross-sectional area, as required for the mechanosensitivity but, by repositioning the membrane-embedded arginines, would also confer sensitivity of MscS to changes in membrane potential. Through this mechanism, the sensitivities of MscS to both applied tension and membrane potential would be coupled, as observed (*1, 9*).

Although TM1 and TM2 appear to be likely candidates for sensing changes in membrane tension or potential, the coupling mechanism between changes in helical orientation and opening and closing of the permeation pathway is less obvious. For ideal, rigid helices arranged with sevenfold symmetry and separated, as for the TM3 helices, by 8 Å, the minimum pore diameter that can be generated is ~10 Å (*33*), close to that observed in the present structure. Consequently, it is unlikely that switching MscS between open and closed states proceeds primarily through reorientation of the helices lining the permeation pathway, as appears to be the dominant contribution for the gating transition of MscL (*15, 18*). Rearrangements of the TM1 and TM2 helices in response to pressure or voltage changes potentially could be propagated to alterations in the TM3 helices either through the residues connecting TM2 and TM3 on the periplasmic surface or perhaps through the cytoplasmic extension of TM3 that is oriented within the membrane plane. Gating the channel in response to these changes could involve distortions or kinking of the helices and associated extramembrane polypeptide, as observed for the calcium-gated, prokaryotic potassium channel (*20, 21*). These conformational transitions could also involve straightening and more complete embedding of TM3 in the membrane (see Fig. 4) as well as deviations from exact rotational symmetry, as also discussed for MscL (*34, 35*). Clearly, more experimental characterization is required to define all the elements involved in gating MscS.

General Implications of the MscS Structure for Channel Gating

Although no sequence homology is evident with other characterized families of ion channels, features of the structural organization of MscS appear to be relevant to the gating mechanism of other channels, particularly mechano- and voltage-sensitive channels.

Mechanosensitivity. Part of the challenge in identifying mechanosensitive channels is that there have been no obvious sequence motifs associated with mechanosensitivity; the diversity of these channels is further emphasized by the lack of structural homology between MscS and MscL. However, as noted in the analysis of *yggB* (*8*), particular membrane-spanning helices in both proteins exhibit a pattern of small (Gly and Ala), conserved residues that tend to be present every fourth residue. These residues, particularly Gly, participate in helix-helix packing interactions [see (*36*)], and, in the structures of MscS and MscL, they are found at the interface positions of the pore-forming helices. These channels exhibit high conductance properties, and this suggests that they both undergo substantial conformational rearrangements in the pore region between the closed and open states, as proposed for MscL (*15, 18*). Consequently, residues at the interface between pore helices must be compatible with helix-packing interactions in both closed and open states. Small amino acids, particularly Gly and Ala, at these positions may facilitate the interconversion between conductance states and hence could be diagnostic for these high-conductance, mechanosensitive channels (*37*).

Voltage gating. The Kv family of voltage-gated potassium channels and the homologous sodium and calcium channels are organized around six transmembrane helices, designated S1 to S6 [see (*3, 22*)]. As established by the structure of the prokaryotic KcsA potassium channel (*12*), the region from S5 to S6 forms the selectivity filter and permeation pathway. The voltage sensitivity of Kv channels is conferred by the S4 helix, which displays a remarkable pattern of about six positive charges, typically arginines, spaced every third residue across the membrane. Likely because of the greater number of membrane-embedded charges in S4, Kv channels are more voltage sensitive than MscS; for the Shaker Kv channel, opening is associated with the equivalent to ~12 charges moving across the membrane. Biophysical and biochemical studies have demonstrated that S4 must be located in "crevices" formed by loose packing against the remainder of the channel, because residues in this helix are accessible to modification by reagents supplied in the external solution [see (*38–40*)]. In response to changes in membrane potential, there is evidence for significant rearrangements in this helix relative to the remainder of the channel [see (*41, 42*)]. Although the structure of the S4 component of Kv channels is not known, there appear to be parallels between the inferred properties of the S4 helix and TM1-TM2 of MscS—namely, the presence of positively charged groups (arginines) in the membrane-spanning region and the relatively loose packing against the remainder of the channel, so that voltage-mediated changes in the positions of these helices can occur and be coupled to opening and closing of the permeation pathway.

Extramembrane domains. Although the transmembrane domains traditionally have been the focus of efforts to understand ion conductance and gating, the extramembrane domains clearly influence these channel properties as well. Structural studies of intact channels by electron microscopy (*29, 43, 44*) and crystallography (*11, 20*) reveal the intimate interactions between membrane-spanning and extramembrane domains that will necessarily influence the permeation pathway for ions to cross the bilayer and also influence the closed-to-open equilibrium at the heart of gating. One consequence of the arrangement of openings and pores in MscS is that the passage of solutes through this channel cannot simply proceed as a "straight shot" across

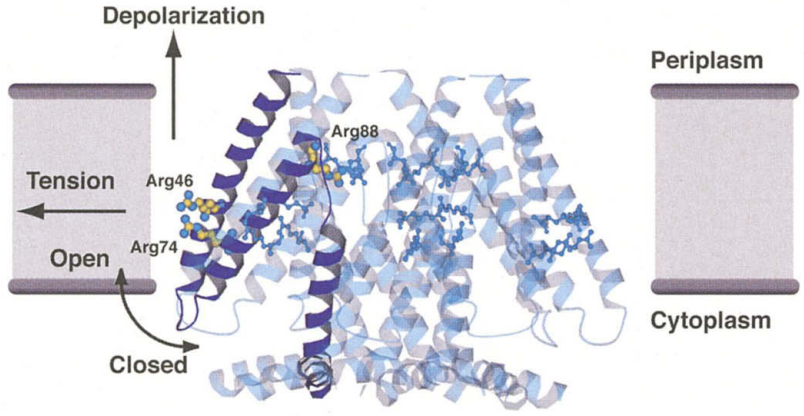

Fig. 4. Model for gating the MscS channel. The transmembrane region of the channel, in an open state, is shown in an expanded view, with one subunit highlighted in dark blue and the remaining six subunits represented in transparent light blue. The side chains of arginine residues at positions 46, 74, and 88 are depicted as larger, colored ball and sticks in the highlighted subunit and as smaller, blue ball and sticks in the remaining subunits. The inferred position of the membrane bilayer is schematically indicated as a gray box. Arrows drawn normal and parallel to the plane of the membrane denote the likely directions of force when depolarization and mechanical stress are applied to the membrane, respectively. Curved arrow schematically illustrates the motion the TM1 and TM2 helices could exhibit in response to either or both of these forces.

the membrane but must involve a more intricate and long-distance flow through extramembrane regions that provide opportunities for regulating channel conductance. The portals, chambers, and vestibules observed in the cytoplasmic domain MscS (Fig. 3) are reminiscent in size and organization of those described for the acetylcholine receptor (*29*), the Shaker potassium channel (*43*), and the sodium channel (*44*). These regions have been suggested to serve as filters that screen out impermeant molecules on the basis of size and perhaps electrostatic factors as well as to provide docking sites for other proteins to regulate conductance properties (*29*).

These resemblances between aspects of the structural organization and functional properties of MscS to other channels reinforce a view that the different elements of channel structure—pore, selectivity filters, sensing modules, and extramembrane domains—can be combined in various ways to create channels with distinctive properties. Over the past few years, increasing progress has been reported in defining the structural arrangements for these elements in prokaryotic channels. The immediate challenge to structural biologists now is to extend these analyses from prokaryotic channels to the more complex systems found in eukaryotes.

References and Notes

1. B. Martinac, M. Buechner, A. H. Delcour, J. Adler, C. Kung, *Proc. Natl. Acad. Sci. U.S.A.* **84**, 2297 (1987).
2. C. Berrier, A. Coulombe, C. Houssin, A. Ghazi, *FEBS Lett.* **259**, 27 (1989).
3. B. Hille, *Ion Channels of Excitable Membranes* (Sinauer Associates, Sunderland, CT, ed. 3, 2001).
4. S. I. Sukharev, P. Blount, B. Martinac, F. R. Blattner, C. Kung, *Nature* **368**, 265 (1994).
5. S. Sukharev, *Biophys. J.* **83**, 290 (2002).
6. C. Berrier, A. Coulombe, I. Szabo, M. Zoratti, A. Ghazi, *Eur. J. Biochem.* **206**, 559 (1992).
7. S. I. Sukharev, P. Blount, B. Martinac, C. Kung, *Annu. Rev. Physiol.* **59**, 633 (1997).
8. N. Levina *et al.*, *EMBO J.* **18**, 1730 (1999).
9. C. Cui, D. O. Smith, J. Adler, *J. Membr. Biol.* **144**, 31 (1995).
10. D. McLaggan *et al.*, *Mol. Microbiol.* **43**, 521 (2002).
11. G. Chang, R. H. Spencer, A. T. Lee, M. T. Barclay, D. C. Rees, *Science* **282**, 2220 (1998).
12. D. A. Doyle *et al.*, *Science* **280**, 69 (1998).
13. S. I. Sukharev, B. Martinac, V. Y. Arshavsky, C. Kung, *Biophys. J.* **65**, 177 (1993).
14. A. Kloda, B. Martinac, *Archaea* **1**, 35 (2002).
15. S. Sukharev, M. Betanzos, C.-S. Chiang, H. R. Guy, *Nature* **409**, 720 (2001).
16. S. Sukharev, S. R. Durell, H. R. Guy, *Biophys. J.* **81**, 917 (2001).
17. E. Perozo, A. Kloda, D. M. Cortes, B. Martinac, *Nature Struct. Biol.* **9**, 696 (2002).
18. E. Perozo, D. M. Cortes, P. Sompornpisut, A. Kloda, B. Martinac, *Nature* **418**, 942 (2002).
19. Y.-S. Liu, P. Sompornpisut, E. Perozo, *Nature Struct. Biol.* **8**, 883 (2001).
20. Y. Jiang *et al.*, *Nature* **417**, 515 (2002).
21. Y. Jiang *et al.*, *Nature* **417**, 523 (2002).
22. F. Bezanilla, *Physiol. Rev.* **80**, 555 (2000).
23. Materials and methods are available as supporting material on *Science* Online.
24. D. C. Rees, G. Chang, R. H. Spencer, *J. Biol. Chem.* **275**, 713 (2000).
25. C. Cui, J. Adler, *J. Membr. Biol.* **150**, 143 (1996).
26. O. S. Smart, J. Breed, G. R. Smith, M. S. Sansom, *Biophys. J.* **72**, 1109 (1997).
27. E. Perozo, A. Kloda, D. M. Cortes, B. Martinac, *J. Gen. Physiol.* **118**, 193 (2001).
28. R. S. Cantor, *J. Phys. Chem. B* **101**, 1723 (1997).
29. A. Miyazawa, Y. Fujiyoshi, M. Stowell, N. Unwin, *J. Mol. Biol.* **288**, 765 (1999).
30. J. Howard, W. M. Roberts, A. J. Hudspeth, *Annu. Rev. Biophys. Biophys. Chem.* **17**, 99 (1988).
31. A. L. Hodgkin, A. F. Huxley, *J. Physiol. (London)* **117**, 500 (1952).
32. K. Okada, P. C. Moe, P. Blount, *J. Biol. Chem.* **277**, 27682 (2002).
33. R. H. Spencer, D. C. Rees, *Annu. Rev. Biophys. Biomol. Struct.* **31**, 207 (2002).
34. Y. Kong, Y. Shen, T. E. Warth, J. Ma, *Proc. Natl. Acad. Sci. U.S.A.* **99**, 5999 (2002).
35. G. Shapovalov, R. Bass, D. C. Rees, H. A. Lester, unpublished data.
36. M. A. Lemmon, D. M. Engelman, *Q. Rev. Biophys.* **27**, 157 (1994).
37. P. Strop, R. B. Bass, D. C. Rees, *Adv. Prot. Chem.* **63** (in press).
38. N. Yang, R. Horn, *Neuron* **15**, 213 (1995).
39. H. P. Larsson, O. S. Baker, D. S. Dhillon, E. Y. Isacoff, *Neuron* **16**, 387 (1996).
40. D. M. Starace, E. Stefani, F. Bezanilla, *Neuron* **19**, 1319 (1997).
41. A. Cha, G. E. Snyder, P. R. Selvin, F. Bezanilla, *Nature* **402**, 809 (1999).
42. K. S. Glauner, L. M. Mannuzzu, C. S. Gandhi, E. Y. Isacoff, *Nature* **402**, 813 (1999).
43. O. Sokolova, L. Kolmakova-Partensky, N. Grigorieff, *Structure* **9**, 215 (2001).
44. C. Sato *et al.*, *Nature* **409**, 1047 (2001).
45. Z. Otwinowski, W. Minor, *Methods Enzymol.* **276**, 307 (1997).
46. T. C. Terwilliger, J. Berendzen, *Acta Crystallogr.* **D55**, 849 (1999).
47. E. de la Fortelle, G. Bricogne, *Methods Enzymol.* **276**, 472 (1997).
48. Collaborative Computational Project No. 4, *Acta Crystallogr.* **D50**, 760 (1994).
49. T. A. Jones, J.-Y. Zou, S. W. Cowan, M. Kjelgaard, *Acta Crystallogr.* **A47**, 110 (1991).
50. A. Brünger *et al.*, *Acta Crystallogr.* **D54**, 905 (1998).
51. R. A. Laskowski, M. W. MacArthur, D. S. Moss, J. M. Thornton, *J. Appl. Crystallogr.* **26**, 283 (1993).
52. P. J. Kraulis, *J. Appl. Crystallogr.* **24**, 946 (1991).
53. E. A. Merritt, D. J. Bacon, *Methods Enzymol.* **277**, 505 (1997).
54. O. S. Smart, J. G. Neduvelil, X. Wang, B. A. Wallace, M. S. Sansom, *J. Mol. Graph.* **14**, 354 (1996).
55. A. Nicholls, K. Sharp, B. Honig, *Proteins Struct. Funct. Genet.* **11**, 281 (1991).
56. A. Nicholls, B. Honig, *J. Comp. Chem.* **12**, 435 (1991).

57. Supported by NIH (D.C.R.) and by a National Service Research Award postdoctoral fellowship (R.B.B.). Discussions with R. Spencer, K. Locher, A. Lee, O. Einsle, D. Dougherty, and H. Lester are greatly appreciated. We thank the staffs at the Advanced Light Source, Advanced Photon Source, National Synchrotron Light Source, and the Stanford Synchrotron Radiation Laboratory (SSRL) facilities for their invaluable assistance. These facilities are funded by the Office of Basic Energy Sciences, U.S. Department of Energy, and NIH. The coordinates have been deposited in the Protein Data Bank (1MXM) for release upon publication.

Supporting Online Material

www.sciencemag.org/cgi/content/full/298/5598/1582/DC1
Materials and Methods
Figs. S1 and S2

30 August 2002; accepted 7 October 2002

Mechanisms of AIF-Mediated Apoptotic DNA Degradation in *Caenorhabditis elegans*

Xiaochen Wang,[1]* Chonglin Yang,[1]* Jijie Chai,[2] Yigong Shi,[2] Ding Xue[1]†

Apoptosis-inducing factor (AIF), a mitochondrial oxidoreductase, is released into the cytoplasm to induce cell death in response to apoptotic signals. However, the mechanisms underlying this process have not been resolved. We report that inactivation of the *Caenorhabditis elegans* AIF homolog *wah-1* by RNA interference delayed the normal progression of apoptosis and caused a defect in apoptotic DNA degradation. WAH-1 localized in *C. elegans* mitochondria and was released into the cytosol and nucleus by the BH3-domain protein EGL-1 in a caspase (CED-3)–dependent manner. In addition, WAH-1 associated and cooperated with the mitochondrial endonuclease CPS-6/endonuclease G (EndoG) to promote DNA degradation and apoptosis. Thus, AIF and EndoG define a single, mitochondria-initiated apoptotic DNA degradation pathway that is conserved between *C. elegans* and mammals.

Programmed cell death (apoptosis) is a fundamental feature in the development and tissue homeostasis of metazoans (*1*, *2*). During apoptosis, the cell activates a suicide machinery that executes orderly cell disassembly, including condensation and fragmentation of the chromosomal DNA (*1*). Many key components that initiate and execute apoptosis are conserved across species (*3*). For example, the onset of apoptosis is controlled by a regulatory pathway involving conserved cell death activators and inhibitors: EGL-1 and BH3-domain-only proteins, CED-9 and Bcl-2, CED-4 and Apaf-1, and CED-3 and caspases, in nematodes

[1]Department of Molecular, Cellular, and Developmental Biology, University of Colorado, Boulder, CO 80309, USA. [2]Department of Molecular Biology, Princeton University, Princeton, NJ 08544, USA.

*These authors contributed equally to this work.
†To whom correspondence should be addressed. E-mail: ding.xue@colorado.edu